

# RSC Advances



This is an *Accepted Manuscript*, which has been through the Royal Society of Chemistry peer review process and has been accepted for publication.

*Accepted Manuscripts* are published online shortly after acceptance, before technical editing, formatting and proof reading. Using this free service, authors can make their results available to the community, in citable form, before we publish the edited article. This *Accepted Manuscript* will be replaced by the edited, formatted and paginated article as soon as this is available.

You can find more information about *Accepted Manuscripts* in the [Information for Authors](#).

Please note that technical editing may introduce minor changes to the text and/or graphics, which may alter content. The journal's standard [Terms & Conditions](#) and the [Ethical guidelines](#) still apply. In no event shall the Royal Society of Chemistry be held responsible for any errors or omissions in this *Accepted Manuscript* or any consequences arising from the use of any information it contains.



Journal Name

ARTICLE

## A novel approach for detection and quantification of magnetic nanomarkers using a spin valve GMR-integrated microfluidic sensor

Received 00th January 20xx,  
Accepted 00th January 20xx

DOI: 10.1039/x0xx00000x

www.rsc.org/

J. Devkota<sup>a,b</sup>, G. Kokkinis<sup>a</sup>, T. Berris<sup>a</sup>, M. Jamalieh<sup>a</sup>, S. Cardoso<sup>c</sup>, F. Cardoso<sup>c</sup>, H. Srikanth<sup>b</sup>, M.H. Phan<sup>b,†</sup> and I. Giouroudi<sup>a,†</sup>

We demonstrate the application of a spin valve giant magneto-resistance (GMR) integrated microfluidic sensor for the detection and quantification of superparamagnetic nanomarkers. A microfluidic channel containing the magnetic fluid, micro-conductors (MCs) for collection of magnetic markers and a spin valve GMR sensor for detecting the presence of magnetic stray field were integrated into a single chip and employed for detection of various concentrations of Nanomag-D beads of 250 nm diameter. The results show that the sensor is capable of detecting concentrations as low as 500 pg/ $\mu$ l of Nanomag-D beads and quantifying them in a linear scale over a wide particle concentration range (1 ng/ $\mu$ l - 500 ng/ $\mu$ l). Our study provides a novel platform towards the development of a portable lab-on-a-chip sensor.

### Introduction

Epidemic and public health care around the globe has an increasing demand of a cost-effective, portable, and user-friendly diagnostic system for an accurate, reliable, and rapid analysis of biological entities to control infectious diseases and pathogens (Aytur et al. 2006; Pejic et al. 2006; Sanvicens et al. 2009). While optical and electrochemical techniques have long been used for medical diagnosis, they are sometimes complex for integration into a chip, require a relatively large amount of reagents, and may possess autofluorescence, absorption, scattering, and possible unwanted reactions (Hahm 2011; Haun et al. 2010; Llandro et al. 2010; Wang and Li 2008). A combination of magnetic sensors with magnetic nanoparticles has provided a promising alternative that can fulfill the increasing requirements of such a portable robust device (Baselt et al. 1998; Devkota et al. 2014; Gaster et al. 2011; Haun et al. 2010; Hua 2013; Kokkinis et al. 2013; Li et al. 2006; Llandro et al. 2010; Wang and Li 2008). These biosensors, in general, utilize the stray fields (Baselt et al. 1998; Wang and Li 2008) or relaxation time (Haun et al. 2010; Koh and Josephson 2009) of functionalized magnetic nanoparticles (also known as magnetic markers) to detect and quantify the bioanalytes tagged to them. Giant magnetoresistance (GMR) biosensors (Baselt et al. 1998; Wang and Li 2008), based on the former principle, have emerged as excellent biosensing techniques for room temperature detection and quantification of biological entities due to their high sensitivity, less complex

instrumentation, compact size, and integration flexibility. Current efforts are to integrate these sensors within microfluidic devices to develop a cost-effective, sensitive, and portable device for rapid diagnosis of diseases (Giouroudi and Keplinger 2013; Sanvicens et al. 2009).

GMR, which refers to a large change in the resistivity of a layered ferromagnetic material subject to an applied DC magnetic field (Baibich et al. 1988; Binasch et al. 1989), is being widely exploited in hard disk drives. However, its applicability to biosensing was not much noticed until Baselt et al. demonstrated, in 1998, the capacity of using an GMR-based sensor for detection of magnetic beads (Baselt et al. 1998). Since then a variety of GMR-based platforms have been developed for sensitive and low-cost biodetection (Baselt et al. 1998; Freitas et al. 2007; Haun et al. 2010; Kokkinis et al. 2013; Li and Kosel 2012; Mark et al. 2010; Wang and Li 2008). In recent years, magnetic tunnelling junction (Li and Kosel 2013; Shen et al. 2008) and spin-valve GMR (Wang and Li 2008) based sensors have gained growing interest over regular GMR and anisotropic MR sensors for their higher detection sensitivity (Llandro et al. 2010). Regardless of the sensor type, the detection of magnetic biomarkers, either single bead or their mass coverage, using a GMR sensor significantly depends upon the measurement conditions. For instance, delivery of a test sample to the sensor by drop casting or open flow injection techniques requires a large amount of sample volume, takes a longer time for the sample to be settled on the sensor surface, and offers no control over the physical motion of the beads that minimizes the chances of the beads reaching to the sensor surface. These effects degrade the biosensors' performance, thus providing limited information about the bio-agents tagged to the beads. In these circumstances, the sensors are also unsafe when working with biothreats, limiting their practical use for epidemic and public health purposes.

<sup>a</sup>Institute of Sensor and Actuator Systems, Vienna University of Technology, Austria

<sup>b</sup>Department of Physics, University of South Florida, USA

<sup>c</sup>INESC Microsistemas y Nanotecnologias, Lisboa, Portugal

† phanm@usf.edu and ioanna.giouroudi@tuwien.ac.at

See DOI: 10.1039/x0xx00000x

On the other hand, microfluidic systems have been developed as a popular pathway in biology and medicine for reliable experiments in a controlled and safe environment (Halldorsson et al. 2015; Mark et al. 2010). This technology has been being widely exploited in a wide range of domains, such as biosensing, cell culturing, miniaturization, and bio-chemical processes (Halldorsson et al. 2015; Mark et al. 2010). For example, Li et al. integrated tunneling magnetoresistive sensors with a microfluidic system containing circular bead concentrators to detect *E. Coli* tagged to Dynabeads® of 2.8  $\mu\text{m}$  diameter (Li et al. 2012; Li and Kosel 2012). Recently, Kokkinis et al. have reported upon the detection of pathogens using the volumetric change of a single micro-bead in a microfluidic biosensing system composed of spin-valve GMR sensors and a set of parallel micro-conductors (MCs) (Kokkinis et al. 2013). These studies have revealed new approaches to integrating GMR-based sensors with microfluidic systems for advanced biosensing. While conventional biosensors require the application of an external magnetic field, these biosensing devices utilize a current flowing through the MC's, thus making the diagnostic system more portable and compatible to modern electronics. While the previous studies were focused mainly on detection of micron-sized biomarkers, labelling of biological identities such as DNA, viruses and cells require the use of magnetic nanobeads or magnetic nanoparticles and thus detection of these nano-sized biomarkers became increasingly important. These have motivated us to develop a novel spin-valve GMR-integrated microfluidic system for such purposes.

In this paper, we report upon the possibility of using this newly developed microfluidic platform as a biosensor for sensitive detection and quantification of Nanomag-D beads of 250 nm in diameter. The nanobeads used, with the protruding amino groups ( $-\text{NH}_2$ ), can be functionalized with the EDC – NHS chemistry (Kokkinis et al. 2013) and thus can be used to tag biological entities (e.g. viruses, microbial pathogens and cells). For that reason, our system can be ideal for use in clinical diagnosis that requires a rapid and reliable analysis of bioagents.

## Materials and Methods

### GMR Sensors and Microfluidic Channels

Four spin valve GMR sensors with dimensions of  $6\ \mu\text{m} \times 2\ \mu\text{m}$  were fabricated on a Si substrate by sputtering  $\text{Al}_2\text{O}_3$  100 nm / Ta 3 nm / NiFe 3.6 nm / MnIr 8.5 nm / CoFe 2.3 nm / Ru 0.8 nm / CoFe 2.3 nm / Cu 3 nm / CoFe 3 nm / NiFe 3.6 nm / Ta 5 nm / and the patterns were defined by an ion milling process. The 300 nm thick GMR electrodes were sputtered to provide an in-plane current flow to the sensing structures. A 300 nm silicon nitride passivation layer was then deposited. On top of the passivated sensors, nine-gold conducting MCs were fabricated using photolithography and sputtering techniques. Each MC had a width of  $10\ \mu\text{m}$  and a thickness of 500 nm, and was separated by  $10\ \mu\text{m}$  from the nearest neighboring MC. This way, two GMR sensors lied below the first MC and two GMR

sensors lied below the last MC. Finally, two PDMS microfluidic channels, a reference and a measurement channel respectively, of  $50\ \mu\text{m}$  height,  $500\ \mu\text{m}$  width, and 50 mm length were fabricated using a negative photoresist mold patterned by a standard photolithography technique and upon which the PDMS was casted, cured, peeled off and placed on top of the MCs. The MCs were used to concentrate the Nanomag-D beads from the inlet to the outlet of the channels thus decreasing the lower limit of the sensor's range. Fig. 1a displays a schematic of the developed GMR microfluidic sensor, with the details of its cross section and the spin-valve GMR structure shown in Fig. 1b. At the inlets and outlets of the reference and measurement channels, fluidic connectors were integrated to inject the magnetic fluid and pump it out after each measurement. Details of the fabrication of spin-valve GMR sensors, MCs, and microfluidic channels have been reported elsewhere (Freitas et al. 2007; Kokkinis et al. 2013).

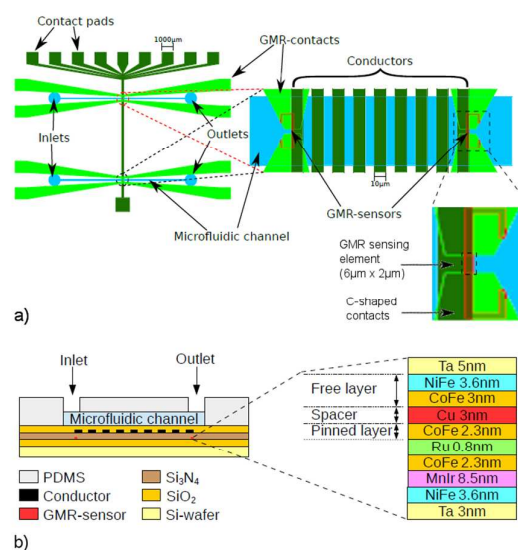


Figure 1. (a) Schematic of the developed GMR microfluidic sensor; one microfluidic channel is used as a reference channel and the second one as the measurement channel; (b) the details of a spin-valve GMR element.

### Magnetic Nanomarkers

In this study, we used commercially available Nanomag-D nanobeads (diameter,  $\sim 250\ \text{nm}$ ) composed of iron oxide nanoparticles encapsulated into a dextran matrix with protruding amino groups ( $-\text{NH}_2$ ). Such nanoparticles can also be purchased with a functionalization layer (e.g. antibodies) in order to tag biological entities (e.g. viruses or microbial pathogens). These nanobeads with an original concentration of  $\sim 10\ \text{mg/mL}$  were purchased from Micromod Partikeltechnologie GmbH, Germany and were diluted to various concentrations in water. A room-temperature magnetic hysteresis (M-H) loop of the nanobeads and their TEM image are shown in Fig. 2 and its inset, respectively. It can be seen in the figure that the M-H loop shows no hysteresis

( $H_c = 0$ ) and no remanence ( $M_r \sim 0$ ), indicating the superparamagnetic characteristic of the nanobeads used. The superparamagnetic nature has been further confirmed by the best fit of the M-H data to the Langevin function. We recall that the superparamagnetic property of magnetic markers is desirable for a variety of biomedical applications (Colombo et al. 2012; Pankhurst et al. 2003).

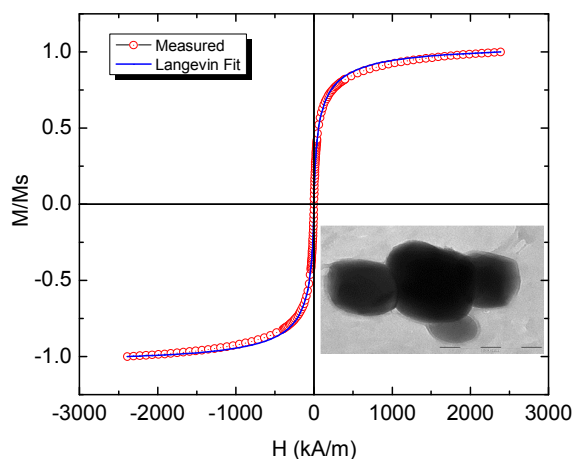


Figure 2. Room temperature magnetic hysteresis loop of Nanomag-D beads. Inset shows a typical TEM image of the particles.

### System Integration and Implementation

In our microfluidic biosensing system, the spin valve GMR sensors and MCs were integrated into a chip and they were covered by the PDMS channels aligned perpendicular to the MCs (Fig. 1a). This configuration allows the magnetic fluid to flow across the MCs. In this study, the desired fluid concentration of Nanomag-D beads was injected to the measurement channel through the inlet and pumped through the outlet for a full coverage of the channel volume. An optical microscope (Nikon-Eclipse LV150) was set up on top of the channel to observe the physical motion of the beads in real time. The MCs were connected to a DC power source of 50 mA (Agilent E3649A Dual output DC power supply) that allowed the beads to be concentrated at the desired MC. In addition, MC #1 was also connected to an AC function generator providing a sinusoidal signal of  $I_M = 10$  mA,  $f_M = 1.234$  kHz (Agilent model 33220A) that was used as a source for an externally applied magnetic field to magnetize the nanobeads. The sensor itself was connected to an AC source of  $I_S = 1$  mA operating at a frequency  $f_S = 0.234$  kHz (Agilent model 33220A) and the voltage across it was measured by a LabVIEW-controlled SR830 Lock-in Amplifier at a locked frequency of  $f_{lock} = f_M + f_S = 1.468$  kHz and a reference voltage of 1V supplied by an Agilent function generator (model 33220A). All three function generators were interconnected and operated at infinite burst mode so as to be in phase. The modulation – demodulation technique using a lock-in amplifier has been described in detail elsewhere (Kokkinis et al, 2014). As the

sensor's transfer curve suggests (Fig. 3) the working point is near the lowest saturation point. This way, even though the sinusoidal voltage output of the sensor decreases, a span of 50 Oe is offered until the sensor is saturated on the upper part of the curve. This way we make sure the upper layering MC's magnetic field, which is of the order of a few Oe, does not saturate the sensor. Finally, all sensors on the chip were of similar characteristics within an insignificant range.

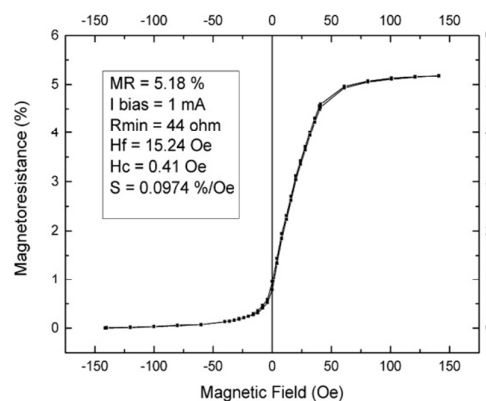


Figure 3. Transfer curve of the integrated GMR sensor.

The Nanomag-D beads, suspended in water, were injected into the channel by placing a droplet in the inlet and applying a sub-pressure in the outlet. Once injected with no additional flow applied (static fluid), the beads were first attracted at MC #8 by a DC magnetic field and then transferred towards the sensor by sequentially applying a current through the consecutive MCs.

The voltage  $V_s$  measured across the GMR sensor was recorded as a function of time and the relative change in voltage was considered as the sensor's figure-of-merit. The relative change in the sensor voltage due to the presence of the magnetic nanobeads on the first MC was defined as the voltage ratio; calculated as

$$\frac{\Delta V}{V} = \frac{|V_0 - V_{sat}|}{V_{sat}} \times 100\% \quad (1)$$

where  $V_0$  is the voltage  $V_s$  across the GMR sensor at  $t = 0$ , i.e. the beads begin to move towards the first MC from their original position and  $V_{sat}$  is the saturation value of  $V_s$ , which is ideally achieved when all the magnetic markers are collected at the vicinity of the sensor i.e. on the surface of the MC #1.

### Results and Discussion

Figure 4a and b show the optical microscopy images of Nanomag-D beads (300 ng/ $\mu$ l) concentrated on MC #2 and MC #1, respectively. The nanobeads were spread throughout the PDMS measurement channel when the magnetic fluid was injected into it. To achieve the highest effect of the nanobeads

on the GMR sensor's voltage  $V_s$ , all of the beads must be collected into a close proximity to the sensor. To achieve that the sample was initially left for two minutes to sediment. With the channels height being  $50\ \mu\text{m}$  and the conductors being able to exert a magnetic force on the beads from a distance of  $30\ \mu\text{m}$  we can confirm that the entire volume of the channel was swept clean from beads at the area above the conductors. Initially the nanobeads were manipulated and collected on the surface of MC # 8 by supplying a DC current of  $I_M = 50\ \text{mA}$ . The DC current applied to the MC induced a magnetic field gradient and hence the magnetic force that pulled the nanobeads onto its surface. Once the nanobeads were collected on MC #8, they were then transferred to MC #7. This process continued until the nanobeads reached MC #3 or #2, followed by the measurement of  $V_s$  across the sensor. The transfer of the nanobeads to each consecutive MC was followed by the  $V_s$  measurement which remained unaffected until the beads reached MC #1. Then, MC #1 was supplied with an AC current as described above and produced a field gradient to the beads on MC #2 or #3 which pulled them towards it. As soon as the beads were collected on the surface of MC #1, as shown in Fig. 4b, the voltage across the GMR sensor started changing. The reduction of  $V_s$  continued until all the beads were collected on the conductor's surface (MC #1). Figure 5(a) shows the sensor voltage ( $V_s$ ) as a function of time ( $t$ ) for water (injected in the reference channel) and Nanomag-D beads (injected in the measurement channel), using the same concentration of  $300\ \text{ng}/\mu\text{l}$ . The OFF and ON states labelled in the figure represent  $I_s = 0, I_M = 0$  and  $I_s \neq 0, I_M \neq 0$  (where  $I_s$  is a current flowing through the sensor and  $I_M$  the current flowing through the conductor), respectively. In this study, the parameter of interest is the "ON" state for which  $V_s$  was recorded as a function of  $t$ . It can be seen that  $V_s$  remained almost unchanged with  $t$  when MC #1 was surrounded by water (reference sensor), indicating a negligible effect of water on  $V_s$ . On the other hand, the  $V_s(t)$  measured for Nanomag-D beads on the surface of MC #1 (measurement sensor) showed a different behavior. Specifically,  $V_s = V_{s,\text{peak}}$  (state – I) was observed immediately after switching on the current ("ON" state) i.e. at  $t = 0$  and then declined with time ( $t > 0$ ) as shown in the first "ON" state for the nanobeads. In the second "ON" state for the nanobeads,  $V_s$  suddenly increased (state – II) and regained the peak value (state – III) when the beads were swiped off the sensor. The peak value (state – III) is similar to the  $V_{s,\text{peak}}$  (state – I) observed at  $t = 0$ .

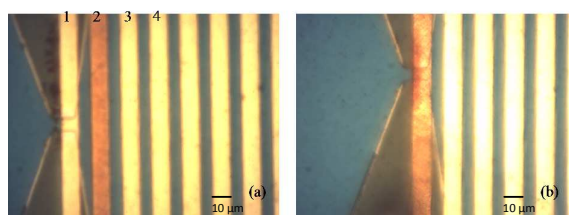


Figure 4. Optical microscopy images of Nanomag-D beads ( $300\ \text{ng}/\mu\text{l}$ ) on the micro-conductors: (a) MC #3 and (b) MC #2.

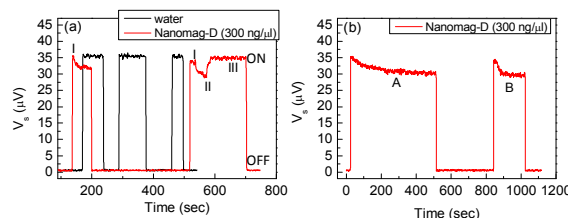


Figure 5. (a) Voltage drop  $V_s$  across the GMR sensor head due to the presence of water and water dispersible Nanomag-D beads of the concentration  $300\ \text{ng}/\mu\text{l}$ . (b)  $V_s$  for Nanomag-D beads transferred to the sensor proximity from different MCs (distance covered for A  $36\ \mu\text{m}$  and for B  $18\ \mu\text{m}$ ).

In real time observation of the motion of nanobeads, none of the nanobeads reached the surface of MC #1 at  $t = 0$ . As a result, the nanobeads induced no effect on the sensor voltage giving the peak value,  $V_{s,\text{peak}}$ . However, as the nanobeads reached the proximity of the sensor head i.e. on the surface of MC #1 for  $t > 0$ ,  $V_s$  started reducing to a lower value. The drop in  $V_s$  was higher for a larger number of nanobeads on the surface of the conductor (MC #1) and the sensor head, but  $V_s$  increased again up to  $V_{s,\text{peak}}$  when the nanobeads were removed from the conductor and the sensor head. When current was supplied to MC #1 for a longer time, so that all the nanobeads were collected on MC #1, the variation in  $V_s$  was observed as shown by the "ON states" in Fig 5(b). It can be observed that with increasing  $t$ ,  $V_s$  first decreased sharply, then slowed down, and finally reached saturation ( $V_{s,\text{sat}}$ ). We define the time required to achieve  $V_{s,\text{sat}}$  as the cutoff time,  $t = t_{\text{cutoff}}$  for a particular measurement.

The falloff of  $V_s$  from  $V_{s,\text{peak}}$  at  $t = 0$  as the nanobeads reached on the surface of MC #1 i.e. approached the proximity of the sensor head. The return of  $V_s$  to a level of  $V_{s,\text{peak}}$  after removing the nanobeads and water from MC #1 indicated that the decrease in  $V_s$  was purely due to the fringe field of the nanobeads. When the nanobeads were present on the surface of the GMR sensor head and/or on the AC-conductor (MC #1), they were magnetized and behaved as magnetic dipoles producing a stray field. This stray field disturbed/super-posed the fields produced by the MC and the sensor itself, thereby modifying the net magnetic field which ultimately altered the orientation of the spins on the free layer of the spin valve sensor from their original directions. This eventually altered the resistance of the sensor that was observed in terms of the decrease in  $V_s$ . At  $t = 0$  and when the nanobeads were swept off the conductor, they were far enough from the sensor head so that the effects of the stray field on the other magnetic fields present on the sensor proximity were negligible. Therefore,  $V_s$  maintained the constant peak level as in the case of water. The decrease in  $V_s$  can be explained by considering the high and low resistance directions of the spin moments. When the nanobeads were present in the proximity of the sensor and on the surface of MC #1, their magnetization was transverse to the sensor/MC length. This caused the magnetic moments in the free layer of the sensor to rotate towards a

low resistance state, causing the decrease in  $V_s$ . With increasing number of nanobeads on the sensor's surface, most magnetic moments were rotated towards a lesser resistance state and  $V_s$  was therefore further decreased. When all the nanobeads reached MC #1 at  $t = t_{\text{cutoff}}$ , there was no further disturbance in the resultant magnetic field on the sensor head to change the angle of the spins so  $V_s$  remained unchanged ( $V_s = V_{s,\text{sat}}$ ).

Thus,  $t_{\text{cutoff}}$  depends upon how fast the nanobeads are collected in the proximity of the sensor for a particular measurement. Ideally the nanobeads should reach the conductor simultaneously as the nanobeads are identical in composition ( $\text{Fe}_3\text{O}_4@\text{Dextran}@-\text{NH}_2$ ) and size (diameter,  $\sim 250$  nm). However, since the width of the MCs ( $w = 10 \mu\text{m}$ ) was fairly large, there was no control for the nanobeads to stick to a particular edge of the MCs. This limited the nanobeads from reaching to MC #1 altogether. Given that the nanobeads were identical and suspended in the same medium and attracted by the same magnetic field gradient, it is possible to estimate the initial position of the nanobeads by knowing  $t_{\text{cutoff}}$  or vice versa. For example, the ON states A and B in Fig. 5(b) show  $V_s$  recorded for the nanobeads transferred to MC #1 from MC #3 and MC #2, respectively. From the figure, one can clearly observe  $t_{\text{cutoff}}$  (A)  $\sim 350$  s, which is about  $4 \times t_{\text{cutoff}}$  (B) ( $\sim 100$  s), while maintaining a similar change in  $V_s$  in both cases. The nominal distances to the centres of MC #2 and MC #3 from the centre of MC #1 were  $d_2 = 18$  and  $d_3 = 36 \mu\text{m}$  (i.e.  $d_3 = 2d_2$ ), respectively. Therefore, the measured value of the respective  $t_{\text{cutoff}}$  could be related to the nanobeads' original point of transfer towards the sensor head. In this case, by doubling the initial position of the nanomarker from the sensor head, the cutoff time increased by about 3.5 times. However, it should be recalled that if the nanobeads are far away from MC #1 such that the field gradient is negligible, they cannot be transferred to the sensor head.

Figure 6 shows  $V_s$  as a function of  $t$  measured for various concentrations in the range of  $1 \text{ ng}/\mu\text{l}$  -  $500 \text{ ng}/\mu\text{l}$  of the magnetic nanobeads. It can be observed that there was a larger drop in  $V_s$  (i.e. smaller values of  $V_{s,\text{sat}}$ ) and a difference in  $t_{\text{cutoff}}$  when increasing the concentration of the nanobeads. The nanobeads of each concentration were transferred from MC #2 to MC #1, as described above, but  $V_s$  took longer time to reach its saturation  $V_{s,\text{sat}}$  in the case of higher concentrations. With increasing concentration of the nanobeads on MC #1, the net stray field was increased; that impacted more the spin moments of the free layer of the sensor, thus leading to a state of lower resistance which ultimately resulted in the lower value of  $V_{s,\text{sat}}$ .

To better quantify the change trend in  $V_s$  with  $t$  with respect to change in the concentration of the nanobeads, we have developed a mathematical formulation to describe  $V_s(t)$  as

$$V_s(t) = Ae^{B/t}, \quad (2)$$

where  $A$  and  $B$  are the fitting parameters. The experimental  $V_s(t)$  data for all the concentrations were fitted using Eq. (2), the representative result of which is shown in Fig. 6b for a given concentration of  $500 \text{ ng}/\mu\text{l}$ . From the best fits,  $A$  and  $B$  were extracted and plotted as functions of the nanobeads'

concentration. We found that while  $A$  remained almost unchanged,  $B$  followed the variation trend of  $t_{\text{cutoff}}$  with increasing concentration of nanobeads. It can be seen in the inset of Fig. 6b that there existed a critical concentration of the nanobeads ( $\sim 150 \text{ ng}/\mu\text{l}$ ), below and above which values of  $B$  and  $t_{\text{cutoff}}$  are remarkably different, denoted as "Regime I" and "Regime II", respectively. Since  $B$  and  $t_{\text{cutoff}}$  are associated with the detection rates of the sensor, such knowledge of their dependences on particle concentration is of practical importance in selecting an optimal particle concentration for rapid biodetection.

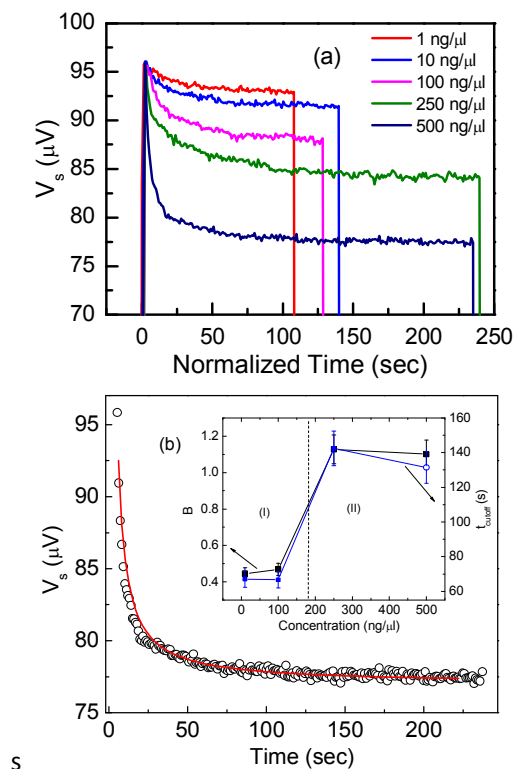


Figure 6. (a) Change in the sensor voltage with accumulation of superparamagnetic Nanomag-D beads on the micro-conductor with respect to the normalized time ( $t$  assumed zero at the beginning of the measurement); (b) The fit to  $V_s(t)$  for Nanomag-D beads of the concentration  $500 \text{ ng}/\mu\text{l}$ . Inset shows variations in the fitting parameter  $B$  and cutoff time with particle concentration and error bars deriving from the fitted curves.

From a biosensing perspective, a good biosensor should be capable of detecting low particle concentrations and effectively quantifying particle concentrations over a large and linear scale (Ahmad et al. 2013). Therefore, in the present study we have calculated the relative change in voltage according to Eq. (1) for various concentrations of Nanomag-D bead, which can be used to tag biomolecules when functionalized. The calculated results and their linear fits are shown in Figure 7. As one can see from this figure,  $\Delta V/V$

increased linearly with the concentration of Nanomag-D beads in the entirely investigated range, from 3.4% for 1 ng/ $\mu$ l to 24.9% for 500 ng/ $\mu$ l.

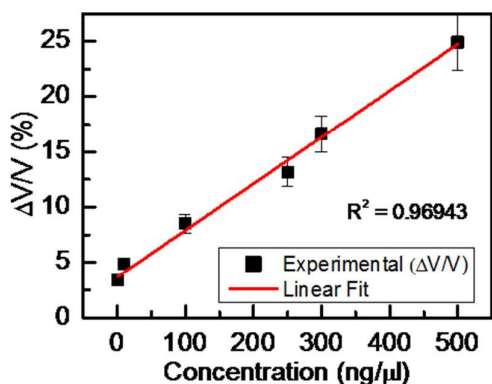


Figure 7. Relative change in the voltage across the GMR sensor head due to the presence of various concentrations of Nanomag-D beads on the MC.

## Conclusions

In this study, we detected particle concentrations as low as 500 pg/ $\mu$ l, quantified them in a linear scale over a wide particle concentration range (1 ng/ $\mu$ l - 500 ng/ $\mu$ l) and measured the sensor voltage for a collection of approximately 20 nanobeads directly above the GMR sensor. We observed a clear decrease in  $V_s$ , and the corresponding  $\Delta V/V$  ratio was determined to be about 1.5%. Our developed sensor also covers a wider linear sensing range in comparison to the range offered by other sensors based on nanoparticles (Devkota et al. 2013; Haun et al. 2010; Rife et al. 2003; Schotter et al. 2002; Wang and Li 2008).

We have proven the application of a spin valve GMR-integrated microfluidic platform for the detection of very low concentrations and quantification of mass coverage of Nanomag-D beads of 250 nm diameter. As several biological identities can be tagged to these nanobeads once they are properly functionalized, the developed sensor has potential for a rapid, portable, and reliable diagnosis of diseases. Experiments are currently being carried out to prove this statement.

## Acknowledgements

Research at the Vienna University of Technology was supported by the Austrian Science Fund (FWF) with Project Nr: P 24372-N19. Research at the University of South Florida was supported by the Florida Cluster for Advanced Smart Sensor Technologies (FCASST) and by USAMRMC through grant

numbers W81XWH-07-1-0708 and W81XWH1020101/3349. JD acknowledges the USF Frank Duckwall Research Fellowship and the Vienna University of Technology Fellowship.

## References

- Ahmad, R., Vaseem, M., Tripathy, N., Hahn, Y.-B., 2013. Wide Linear-Range Detecting Nonenzymatic Glucose Biosensor Based on CuO Nanoparticles Inkjet-Printed on Electrodes. *Analytical Chemistry* 85(21), 10448-10454.
- Aytur, T., Foley, J., Anwar, M., Boser, B., Harris, E., Beatty, P.R., 2006. A novel magnetic bead bioassay platform using a microchip-based sensor for infectious disease diagnosis. *J Immunol Methods* 314(1-2), 21-29.
- Baibich, M.N., Broto, J.M., Fert, A., Vandau, F.N., Petroff, F., Eitenne, P., Creuzet, G., Friederich, A., Chazelas, J., 1988. Giant magnetoresistance of (001)Fe/(001)Cr magnetic superlattices. *Phys. Rev. Lett.* 61(21), 2472-2475.
- Baselt, D.R., Lee, G.U., Natesan, M., Metzger, S.W., Sheehan, P.E., Colton, R.J., 1998. A biosensor based on magnetoresistance technology. *Biosens Bioelectron* 13(7-8), 731-739.
- Binasch, G., Grünberg, P., Saurenbach, F., Zinn, W., 1989. Enhanced magnetoresistance in layered magnetic structures with antiferromagnetic interlayer exchange. *Physical Review B* 39(7), 4828-4830.
- Colombo, M., Carregal-Romero, S., Casula, M.F., Gutierrez, L., Morales, M.P., Bohm, I.B., Heverhagen, J.T., Prospero, D., Parak, W.J., 2012. Biological applications of magnetic nanoparticles. *Chem Soc Rev* 41(11), 4306-4334.
- Devkota, J., Mai, T.T.T., Stojak, K., Ha, P.T., Pham, H.N., Nguyen, X.P., Mukherjee, P., Srikanth, H., Phan, M.H., 2014. Synthesis, inductive heating, and magnetoimpedance-based detection of multifunctional Fe3O4 nanoconjugates. *Sensor Actuat B-Chem* 190, 715-722.
- Devkota, J., Wang, C., Ruiz, A., Mohapatra, S., Mukherjee, P., Srikanth, H., Phan, M., 2013. Detection of low-concentration superparamagnetic nanoparticles using an integrated radio frequency magnetic biosensor. *J Appl Phys* 113(10), 104701.
- Freitas, P.P., Ferreira, R., Cardoso, S., Cardoso, F., 2007. Magnetoresistive sensors. *J Phys-Condens Mat* 19(16) 165221.
- Gaster, R.S., Xu, L., Han, S.J., Wilson, R.J., Hall, D.A., Osterfeld, S.J., Yu, H., Wang, S.X., 2011. Quantification of protein interactions and solution transport using high-density GMR sensor arrays. *Nat Nanotechnol* 6(5), 314-320.
- Giouroudi, I., Keplinger, F., 2013. Microfluidic Biosensing Systems Using Magnetic Nanoparticles. *Int J Mol Sci* 14(9), 18535-18556.
- Hahn, J.-i., 2011. Functional polymers in protein detection platforms: Optical, electrochemical, electrical, mass-sensitive, and magnetic biosensors. *Sensors-Basel* 11(3), 3327-3355.
- Halldorsson, S., Lucumi, E., Gomez-Sjoberg, R., Fleming, R.M.T., 2015. Advantages and challenges of microfluidic cell culture in polydimethylsiloxane devices. *Biosens Bioelectron* 63, 218-231.
- Haun, J.B., Yoon, T.J., Lee, H., Weissleder, R., 2010. Magnetic nanoparticle biosensors. *Wires Nanomed Nanobi* 2(3), 291-304.
- Hua, W., 2013. Magnetic Sensors for Diagnostic Medicine: CMOS-Based Magnetic Particle Detectors for Medical Diagnosis Applications. *Microwave Magazine, IEEE* 14(5), 110-130.
- Koh, I., Josephson, L., 2009. Magnetic Nanoparticle Sensors. *Sensors-Basel* 9(10), 8130-8145.

- 17 Kokkinis, G., Keplinger, F., Giouroudi, I., 2013. On-chip microfluidic biosensor using superparamagnetic microparticles. *Biomicrofluidics* 7(5) 054117.
- 18 Li, F.Q., Giouroudi, I., Kosel, J., 2012. A biodetection method using magnetic particles and micro traps. *J Appl Phys* 111(7) 07B328.
- 19 Li, F.Q., Kosel, J., 2012. A Magnetic Method to Concentrate and Trap Biological Targets. *IEEE Trans Magn* 48(11), 2854-2856.
- 20 Li, F.Q., Kosel, J., 2013. A Magnetic Biosensor System for Detection of *E. coli*. *IEEE Trans Magn* 49(7), 3492-3495.
- 21 Li, G.X., Sun, S.H., Wilson, R.J., White, R.L., Pourmand, N., Wang, S.X., 2006. Spin valve sensors for ultrasensitive detection of superparamagnetic nanoparticles for biological applications. *Sensor Actuat a-Phys* 126(1), 98-106.
- 22 Llandro, J., Palfreyman, J.J., Ionescu, A., Barnes, C.H.W., 2010. Magnetic biosensor technologies for medical applications: a review. *Med Biol Eng Comput* 48(10), 977-998.
- 23 Mark, D., Haeberle, S., Roth, G., von Stetten, F., Zengerle, R., 2010. Microfluidic lab-on-a-chip platforms: requirements, characteristics and applications. *Chem Soc Rev* 39(3), 1153-1182.
- 24 Pankhurst, Q.A., Connolly, J., Jones, S.K., Dobson, J., 2003. Applications of magnetic nanoparticles in biomedicine. *J Phys D Appl Phys* 36(13), R167-R181.
- 25 Pejic, B., De Marco, R., Parkinson, G., 2006. The role of biosensors in the detection of emerging infectious diseases. *Analyst* 131(10), 1079-1090.
- 26 Rife, J.C., Miller, M.M., Sheehan, P.E., Tamanaha, C.R., Tondra, M., Whitman, L.J., 2003. Design and performance of GMR sensors for the detection of magnetic microbeads in biosensors. *Sensors and Actuators A: Physical* 107(3), 209-218.
- 27 Sanvicens, N., Pastells, C., Pascual, N., Marco, M.P., 2009. Nanoparticle-based biosensors for detection of pathogenic bacteria. *Trac-Trend Anal Chem* 28(11), 1243-1252.
- 28 Schotter, J., Kamp, P.B., Becker, A., Puhler, A., Brinkmann, D., Schepper, W., Bruckl, H., Reiss, G., 2002. A biochip based on magnetoresistive sensors. *IEEE Trans Magn* 38(5), 3365-3367.
- 29 Shen, W., Schrag, B.D., Carter, M.J., Xie, J., Xu, C., Sun, S., Xiao, G., 2008. Detection of DNA labeled with magnetic nanoparticles using MgO-based magnetic tunnel junction sensors. *J Appl Phys* 103(7), - 07A306.
- 30 Wang, S.X., Li, G., 2008. Advances in giant magnetoresistance biosensors with magnetic nanoparticle tags: Review and outlook. *IEEE Trans Magn* 44(7), 1687-1702.